Journal of Materials Chemistry C

ROYAL SOCIETY OF CHEMISTRY

PAPER

View Article Online
View Journal

Cite this: DOI: 10.1039/d5tc04017e

Effect of deuteration on exciplex dynamics in organic donor–acceptor blends

Yuto Nagasaki,[a] Hajime Nakanotani *[b] and Chihaya Adachi *[ac]

Received 12th November 2025,
Accepted 20th December 2025

DOI: 10.1039/d5tc04017e

rsc.li/materials-c

Exciplex systems based on deuterated organic semiconducting molecules provide a promising strategy to enhance the performance of organic light-emitting diodes (OLEDs). Although the enhancement of OLED performance by utilizing a partially deuterated exciplex system has been reported, the impact of deuteration of the organic semiconducting molecule on exciplex dynamics has not been fully characterized. Here, we investigate the impact of deuteration of the electron-donor molecules (**mCP-d_{20}**: 1,3-dicarbazole-benzene-d_{20}) on the exciplex dynamics in the **mCP-d_{20}**: 2,4,6-tris[3-(diphenylphosphinyl)phenyl]-1,3,5-triazine (**PO-T2T**) co-deposited films. Compared to the co-deposited films based on undeuterated **mCP**, the **mCP-d_{20}**:**PO-T2T** films exhibited a 1.5-fold increase in photoluminescence quantum yield (PLQY) with prolonged delayed emission lifetime. Temperature-dependent kinetic analyses for electron transition processes revealed that the enhancement of PLQY in the **mCP-d_{20}**:**PO-T2T** films originates from the suppression of thermally activated nonradiative decay from the excited charge-transfer triplet state by donor deuteration. Consequently, the OLED based on the deuterated exciplex system demonstrated a higher external quantum efficiency than those employing undeuterated donors.

Introduction

Organic light-emitting diodes (OLEDs) have garnered significant attention as a key technology for next-generation display applications due to their outstanding features, including ultra-high flexibility, lightweight design, and the potential for low-cost manufacturing. Although OLED displays have been commercialized in various fields, a further improvement of OLED performance, such as simultaneously achieving low driving voltage, high external electroluminescence (EL) quantum efficiency (EQE), and stable OLED operation even at ultra-high current densities, is essential for advancing high-performance OLED-based applications, such as ultra-dense micro-OLED displays to support future AR/VR technologies.

According to spin statistics, the electron spin states of the excitons formed *via* charge recombination events in OLEDs follow the branching ratio of 1 : 3, yielding the lowest singlet (S_1) and triplet (T_1) excited states, respectively. Since the radiative decay transition from the T_1 state to the ground state (S_0) is generally a spin-forbidden process, to harvest the T_1 energy as bright EL, the use of room-temperature phosphorescent materials containing heavy atoms and/or thermally activated delayed fluorescence (TADF) molecules has been widely investigated.[1–4] In particular, the use of TADF molecules has attracted much attention because TADF molecules can serve not only as emitters but also as triplet energy harvesters in OLEDs, *i.e.*, hyperfluorescence, leading to a highly efficient EL with a narrow EL spectrum.[5]

In the TADF process, minimizing the S_1–T_1 energy gap (ΔE_{ST}) is a fundamental key parameter for realizing efficient spin conversion because the reverse intersystem crossing (RISC) rate constant (k_{RISC}) from the T_1 to the S_1 state is inversely proportional to ΔE_{ST}. To reduce the ΔE_{ST} to a level similar to thermal energy at room temperature, the spatial overlap between the highest occupied molecular orbital (HOMO) and the lowest unoccupied molecular orbital (LUMO) should be carefully minimized. For an ideal TADF process, molecular design strategies frequently employ either intramolecular charge-transfer (CT)-type excited states or intermolecular CT-type excited states. In both cases, when the T_1 energy levels of the electron-donor and electron-acceptor units, *i.e.*, localized T_1 state, lie above the CT-type excited T_1 state, the S_1 and T_1 states of the molecular system should have strong CT character, resulting in the formation of the lowest CT-type excited S_1 and T_1 states (^{1}CT and ^{3}CT) with small ΔE_{ST}. Since the small spatial overlap between the HOMO and LUMO can effectively minimize ΔE_{ST}, exciplexes (intermolecular

[a] *Center for Organic Photonics and Electronics Research (OPERA), Kyushu University, Motooka, Nishi, Fukuoka 819-0395, Japan. E-mail: adachi@cstf.kyushu-u.ac.jp*
[b] *Research Institute for Electronic Science, Hokkaido University, N20W10, Kita, Sapporo 001-0020, Japan. E-mail: nakanotani@es.hokudai.ac.jp*
[c] *International Institute for Carbon Neutral Energy Research (WPI-I2CNER), Kyushu University, 744 Motooka, Nishi, Fukuoka 819-0395, Japan*

excited-state complexes) are among the promising molecular systems for efficient TADF.[6] In addition, unlike intramolecular TADF systems, a TADF-exciplex is generally composed of two distinct materials, *i.e.*, a hole-transport material (electron donor) and an electron-transport material (electron acceptor). The donor–acceptor blend not only provides greater molecular tunability but also has the potential to reduce the driving voltage of OLEDs by alleviating charge-injection barriers during operation. In particular, numerous studies have reported the application of TADF-type exciplexes as emissive or host layers in OLEDs.[6–10]

In addition to the use of efficient TADF-type exciplexes, deuteration of organic molecules has recently attracted significant attention to enhance both EL efficiency and operational stability in OLEDs. Since molecular vibrations, such as C–H stretching modes, are thought to promote nonradiative decay from the excited state to the ground state, lowering their vibrational frequencies by deuteration can be an effective way to suppress nonradiative decay. The improvements in photoluminescence quantum yield (PLQY) resulting from deuteration of emissive molecules have already been reported for several organic molecular systems.[11–16] In addition to the PLQY improvement by deuteration, prolonged OLED operational lifetime has also been reported and is understood to originate from the kinetic isotope effect resulting from hydrogen's mass doubling upon replacement with deuterium.[17–21] Since bond dissociation mediated by radical species or high-energy excited states generated during OLED operation is considered a major cause of device degradation, reducing the rates of such chemical reactions can improve the operational stability. For example, recent studies have demonstrated that complete substitution of hydrogen with deuterium in deep-blue TADF emitters suppresses high-energy C–H bond vibrations and extends their OLED operational lifetime.[15]

A synergistic approach combining both the features of TADF-type exciplexes and the deuteration of organic semiconducting molecules should therefore be a promising strategy for the further development of high-performance OLEDs. Although a pioneering work of deuterated TADF-type exciplexes has been reported by W. Yuan *et al.*,[22] detailed photophysical analysis, such as the concentration dependence of deuterated molecules on the TADF-type exciplex dynamics and rate constant analysis based on the temperature dependence of the exciplex dynamics to unveil the impact of molecular deuteration on the TADF-type exciplex characteristics, has not been fully investigated. Therefore, a comprehensive understanding of the impact of deuteration on the OLED performance in TADF-type exciplexes is required. Here, we investigate the impact of the deuteration of the electron-donor molecules on the exciplex emission properties in the electron donor : acceptor co-deposited films using 1,3-dicarbazole-benzene (**mCP**) and its deuterated analogue **mCP-d_{20}** as the electron donor together with the electron acceptor molecule 2,4,6-tris[3-(diphenylphosphinyl)phenyl]-1,3,5-triazine (**PO-T2T**). It was revealed that a nonradiative decay process from the T_1 state was significantly suppressed in the **mCP-d_{20} : PO-T2T** co-deposited film even at room temperature. The suppression of nonradiative decay was found to become more significant as the fraction of **mCP-d_{20}** increased in the **mCP : PO-T2T** co-deposited films, leading to an increase in PLQY from 23 ± 2% (**mCP : PO-T2T**) to 34 ± 2% (**mCP-d_{20} : PO-T2T**) with extended delayed fluorescence lifetime in **mCP-d_{20} : PO-T2T** (9 : 1). Consequently, the maximum external quantum efficiency (EQE) of OLEDs based on the exciplex was improved from 5.5% (**mCP : PO-T2T**) to 6.4% (**mCP-d_{20} : PO-T2T**). This study elucidates the photophysical processes of an exciplex incorporating deuterated molecules, providing significant insights into the development of stable, high-efficiency exciplex-based systems.

Results and discussion

In this study, we used **mCP-d_{20}** as a deuterated electron donor, which was synthesized according to the previously reported procedure.[16] First, to evaluate the fundamental characteristics of the exciplex formed between **mCP** (or **mCP-d_{20}**) and **PO-T2T** (Fig. 1a), UV-visible absorption and photoluminescence (PL) spectra were measured for pure 50 nm-thick deposited films (**mCP**, **mCP-d_{20}**, and **PO-T2T**) and for the **mCP** (or **mCP-d_{20}**) : **PO-T2T** co-deposited films (50 nm) with a mixing ratio of 90 mol% **mCP** (or **mCP-d_{20}**) and 10 mol% **PO-T2T**. We also characterize the PL properties of a 50 wt% **PO-T2T** : polymethyl methacrylate (PMMA) spin-coated film (Fig. 1b and c). The absorption spectra of **mCP** and **mCP-d_{20}** films exhibited multiple absorption bands between 250 and 340 nm, while a **PO-T2T** film showed an absorption band with a peak around 270 nm. In the co-deposited films, only the absorption features attributable to **mCP**, **mCP-d_{20}**, and **PO-T2T** were observed, indicating the absence of CT interactions between **mCP**/**mCP-d_{20}** and **PO-T2T** in the ground state. Although a broad emission band centered around 520 nm was observed in the pure **PO-T2T** film (Fig. S1), it was not observed in the **PO-T2T** : PMMA film, suggesting that the broad emission originates from the excimer formation between neighboring **PO-T2T** molecules. Furthermore, a distinct emission band centered around 400 nm was observed exclusively in the **mCP** neat film. Since the emission has a nanosecond time scale, it should be attributed not to room-temperature phosphorescence but to the emission from *J*-aggregated **mCP** molecules.[23] Interestingly, such emission was not observed in the **mCP-d_{20}** neat film, likely due to differences in molecular packing in the **mCP-d_{20}** film, supported by the difference in the single crystal structure.[16] Although there is no clear CT interaction in the ground state, the PL spectra of the **mCP : PO-T2T** and **mCP-d_{20} : PO-T2T** co-deposited films exhibit a broad and featureless emission band with a peak wavelength of around 480 nm, distinct from the emission of pure **mCP**, **mCP-d_{20}**, or **PO-T2T** films. The emission energy (~2.6 eV) calculated from the peak emission wavelength corresponds well to the energy difference between the HOMO of **mCP**/**mCP-d_{20}** (−6.1 eV) and the LUMO of **PO-T2T** (−3.5 eV), consistent with the previously reported spectra of **mCP : PO-T2T** thin films,[24] indicating the formation of exciplexes between

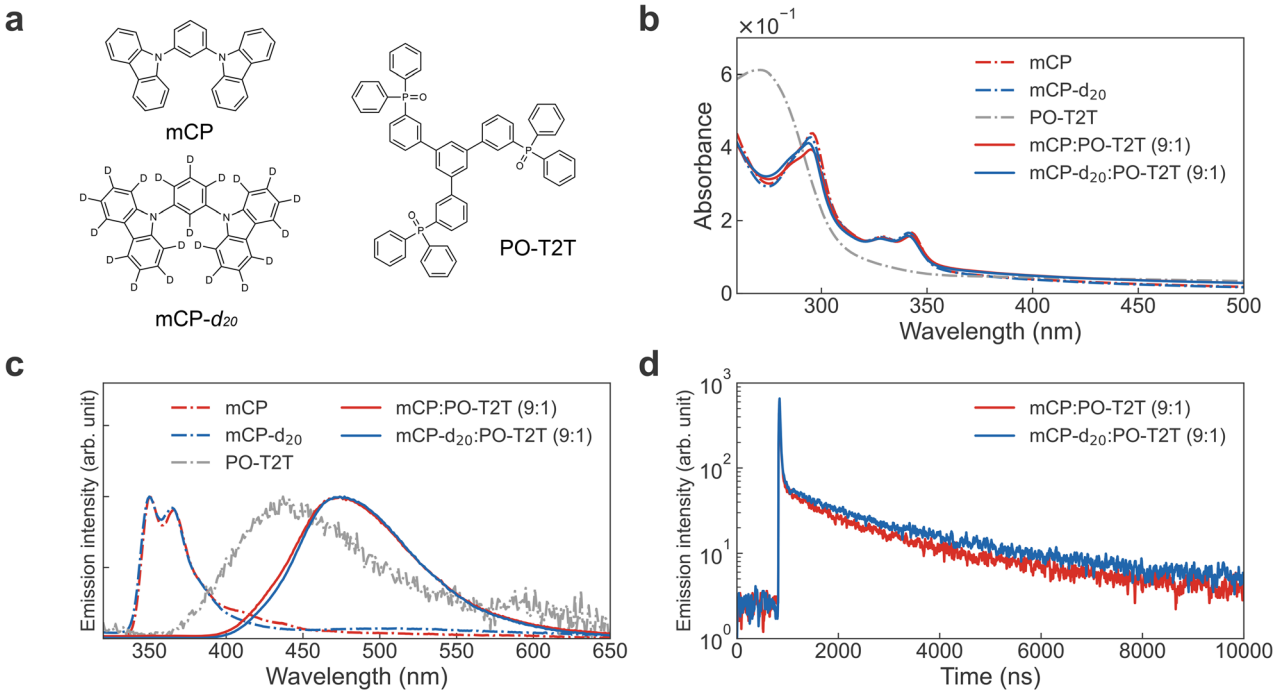

Fig. 1 (a) Chemical structures of the molecules used in this study. (b) Steady-state absorption spectra and (c) PL spectra of **mCP**, **mCP-*d*$_{20}$**, **PO-T2T** : PMMA (50 wt%), and **mCP**/**mCP-*d*$_{20}$** : **PO-T2T**(9 : 1). (d) Transient PL profiles of the **mCP** : **PO-T2T** and **mCP-*d*$_{20}$** : **PO-T2T** co-deposited films (9 : 1) at room temperature.

mCP (or **mCP-*d*$_{20}$**) and **PO-T2T** molecules. The **mCP-*d*$_{20}$: PO-T2T** co-deposited film completely shares the PL spectrum with that of the **mCP : PO-T2T** co-deposited film, indicating that the deuteration of **mCP** did not affect the exciplex emission spectra of the co-deposited films, and similar results were obtained in the **mCP** (or **mCP-*d*$_{20}$**) **: PO-T2T** co-deposited film with various donor-to-acceptor ratios (Fig. S2a and b and Table S1). Collectively, these results demonstrate that deuteration of **mCP** does not affect the energy levels involved in exciplex emission.

To investigate the impact of deuteration on electron-donor molecules on exciplex dynamics, transient PL profiles (Fig. 1d and Fig. S3) and PLQYs were measured for each co-deposited film. Table 1 summarizes the emission decay lifetimes and PLQYs of **mCP** (or **mCP-*d*$_{20}$**) **: PO-T2T** co-deposited films with various donor–acceptor ratios (from 1 : 9 to 9 : 1), as well as the radiative decay rate constant from S_1 (k_r^S), nonradiative decay rate constants from S_1 and T_1 (k_{nr}^S and k_{nr}^T), and the rate constants for ISC and RISC (k_{ISC} and k_{RISC}). All rate constants were calculated using a previously reported analytical method.[25] Compared with the **mCP : PO-T2T** co-deposited films, the **mCP-*d*$_{20}$: PO-T2T** co-deposited films tended to have prolonged delayed fluorescence lifetimes. Furthermore, the PLQYs of **mCP-*d*$_{20}$: PO-T2T** co-deposited (9 : 1 and 7 : 3) films show a clear enhancement compared with those of the **mCP : PO-T2T** co-deposited films. Kinetic analysis revealed that **mCP-*d*$_{20}$** increased the radiative decay rate constant and decreased the nonradiative decay rate constant. This change was particularly pronounced in the co-deposited films with a ratio of 9 : 1, where k_r^S increased from 2.3×10^6 s^{-1} to 2.8×10^6 s^{-1}, while k_{nr}^S decreased from 7.7×10^6 s^{-1} to 5.4×10^6 s^{-1} and k_{nr}^T decreased from 4.8×10^5 s^{-1} to 3.6×10^5 s^{-1}. Note that the ISC and RISC rate constants remained essentially unchanged in all films, indicating that the deuteration of the donor molecules does not affect the spin-flip processes. Based on these experimental

Table 1 Photophysical properties and rate constants for each process of the exciplex

Doped film	τ_p (ns)		τ_d (μs)		PLQY (%)		k_r^S ($\times 10^6$ s^{-1})		k_{nr}^S ($\times 10^6$ s^{-1})		k_{nr}^T ($\times 10^5$ s^{-1})		k_{ISC} ($\times 10^7$ s^{-1})		k_{RISC} ($\times 10^6$ s^{-1})	
mCP/mCP-*d*$_{20}$: PO-T2T	*h*	*d*	*h*	*d*	*h*	*d*	*h*	*d*	*h*	*d*	*h*	*d*	*h*	*d*	*h*	*d*
1 : 9	24	25	3.0	3.2	38 ± 3	38 ± 4	1.1	1.2	1.8	1.8	2.1	2.0	3.8 ± 0.3	3.6 ± 0.3	4.6 ± 0.1	4.1 ± 0.1
3 : 7	25	26	2.9	2.8	37 ± 2	42 ± 3	1,3	1.8	2.3	2.5	2.2	2.2	3.6 ± 0.3	3.4 ± 0.3	3.7 ± 0.1	3.1 ± 0.1
5 : 5	25	24	2.3	2.6	41 ± 3	40 ± 1	2.4	2.2	3.5	3.3	2.7	2.5	3.5 ± 0.3	3.7 ± 0.3	2.8 ± 0.1	2.9 ± 0.1
7 : 3	24	23	2.5	2.5	36 ± 1	43 ± 3	2.1	2.5	3.8	3.3	2.7	2.4	3.7 ± 0.3	3.7 ± 0.3	2.8 ± 0.1	2.9 ± 0.1
9 : 1	21	21	1.7	2.0	23 ± 2	34 ± 2	2.3	2.8	7.7	5.4	4.8	3.6	4.1 ± 0.5	4.1 ± 0.4	2.6 ± 0.2	2.8 ± 0.2

τ_P: lifetime of the prompt component; τ_d: lifetime of the delayed component; k_r^S: rate constant for radiative decay from the singlet excited state; k_{nr}^S: maximum rate constant for nonradiative decay from the singlet excited state; k_{nr}^T: maximum rate constant for nonradiative decay from the triplet excited state; k_{ISC}: average rate constant for the ISC process; k_{RISC}: average rate constant for the RISC process.

results, deuteration of **mCP** suppresses nonradiative decay, resulting in longer delayed fluorescence lifetimes and higher PLQYs.

Previous studies have shown that simultaneous deuteration of both host and guest molecules in thin films suppresses molecular vibrations in the solid state, thereby reducing vibration-induced exciton quenching.[16] A similar effect is observed in the exciplex system studied here, where donor deuteration results in comparable suppression of nonradiative deactivation for both singlet and triplet excited states. Furthermore, this trend became more pronounced as the fraction of **mCP-d_{20}** increased in the co-deposited films. In particular, for the films with 90% **mCP-d_{20}**, the PLQY increased significantly from 23 ± 2% to 34 ± 2% and the τ_d value simultaneously increased from 1.7 μs to 2.0 μs. Obviously, the emissive species in the co-deposited films were identified as the **mCP : PO-T2T** or **mCP-d_{20} : PO-T2T** exciplex, and this assignment should remain consistent for all concentrations. These results therefore highlight that not only the deuteration of emissive species but also that of the surrounding environment is critical for more effective suppression of nonradiative decay. Collectively, these results indicate that increasing the ratio of deuterated donor molecules in the films can effectively suppress vibrational motion and nonradiative decay, thereby enhancing the PLQY of exciplex emission.

To further investigate the effects of donor deuteration on the exciplex emission properties, we examined the temperature dependence of the transient PL characteristics and PLQY in **mCP : PO-T2T** or **mCP-d_{20} : PO-T2T** films with a donor-to-acceptor ratio of 9 : 1. The results are summarized in Fig. 2 and Fig. S4 and Tables S2 and S3. In both films, slightly blueshifted steady-state PL spectra were observed with decreasing temperature (Fig. S4). The delayed emission spectra exhibit a blueshift with decreasing temperature, whereas the prompt emission spectra remain unchanged with varying temperature (Fig. S5). This indicates that the blueshifted emission at steady state is due to the blueshift of the delayed emission component. The delayed emission has an energy of approximately 2.95 eV (Fig. S5c and d), whereas previous studies reported T_1 energies of 3.65 eV for **mCP**[23] and 3.1 eV for **PO-T2T**[26]. Therefore, the delayed emission is unlikely to originate from the phosphorescence of the T_1 states of the donor, acceptor, or exciplex. Rather, this phenomenon indicates that energy stabilization in both the singlet and triplet excited states is restricted at lower temperatures, leading to changes in the spectra of delayed emission.

Interestingly, the PLQY of the exciplex was increased significantly with decreasing temperature. The temperature dependence in the total, delayed, and prompt components of the PLQY is summarized in Fig. 2. Here, the PLQY values at each temperature were estimated from the integrated PL spectral ratios relative to the absolute PLQY value measured at room temperature. As shown in Fig. 2a, the PLQY for total emission in the **mCP** (or **mCP-d_{20}**) : **PO-T2T** (9 : 1) film rapidly increases with decreasing temperature (300–200 K) and then exhibits almost no temperature dependence in the low-temperature region (200–100 K). Furthermore, a similar increase of PLQY in an exciplex system (TCTA : B4PYMPM) has previously been reported,[27] but we find that the **mCP-d_{20} : PO-T2T** system

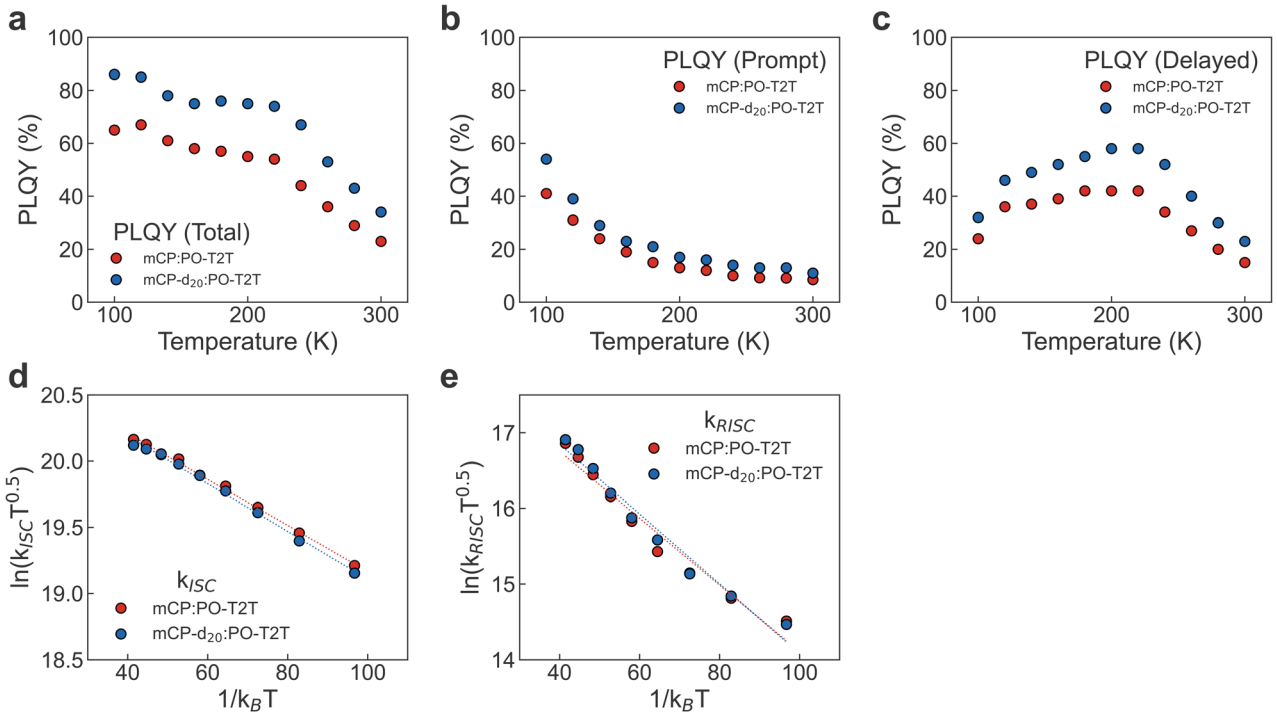

Fig. 2 Temperature dependence of PLQY for (a) total emission, (b) the prompt emission component, and (c) the delayed emission component in the **mCP/mCP-d_{20} : PO-T2T**(9 : 1) co-deposited film. The Marcus plot and activation energy for (d) ISC and (e) RISC rate constants in **mCP/mCP-d_{20} : PO-T2T**(9 : 1).

exhibits a strong temperature dependence in the PLQY for prompt and delayed emission components, as shown in Fig. 2b and c. The PLQY for the prompt component significantly increases with decreasing temperature below 200 K, indicating a temperature-dependent ISC process in the **mCP-d_{20} : PO-T2T** system. Although both systems exhibit similar temperature dependence in the PLQY, the total PLQY in the **mCP-d_{20} : PO-T2T** (9 : 1) film reached 85% at 100 K, while the **mCP : PO-T2T** (9 : 1) film shows a low PLQY (63%), highlighting the impact of the deuteration of **mCP** molecules. Fig. S6 shows the temperature dependence on the PLQY enhancement factor of deuteration obtained by dividing the PLQY of **mCP-d_{20} : PO-T2T** by that of **mCP : PO-T2T**. The enhancement of the PLQY for the delayed component due to donor deuteration was most significant at 300 K and progressively decreased as the temperature decreased. This result indicates that donor deuteration enhances the delayed PLQY at 300 K, where nonradiative decay is highly active. In contrast, at 100 K, where the nonradiative decay process should naturally be suppressed according to the low temperature, the deuteration effect becomes less significant. Furthermore, the PLQY enhancement of the prompt component showed little temperature dependence. Based on these results, we conclude that the donor deuteration effectively suppresses the nonradiative decay process from the triplet excited state more effectively.

Here, we discuss the ISC and RISC processes in the exciplex system. As discussed above, the PLQY for both prompt and delayed emission components increases with decreasing temperature. To understand these behaviors, the activation energies for both ISC and RISC rate constants were evaluated (Fig. 2d and e). Although it is generally believed that an exciplex system has nearly zero ΔE_{ST} because of the significant spatial separation of the HOMO and LUMO, we found that both rate constants exhibit an activation energy. For the ISC and RISC processes, endothermic processes with activation energies of approximately 10 and 46 meV, as calculated from the Marcus plot for k_{ISC} and k_{RISC}, were estimated, respectively. According to the endothermic process, the ISC process should be suppressed at low temperature, leading to the enhancement of the PLQY for the prompt emission component, *i.e.*, radiative decay from the S_1 state. In fact, the PLQY for the prompt component reached 55% at 100 K in the **mCP-d_{20} : PO-T2T** (9 : 1) film, which is almost five times higher than that at room temperature. On the other hand, the PLQY for the delayed emission component reaches its maximum around 200–220 K (PLQY = 58% at 200 K) and tends to decrease with a further decrease in temperature (200–100 K). Generally, the TADF process should be suppressed by decreasing the temperature. However, the **mCP-d_{20} : PO-T2T** exciplex systems exhibit a clear increase in the PLQY for the delayed component, indicating a significant impact of a vibrationally induced nonradiative decay process on the PLQY in the high-temperature range (300–200 K). On the other hand, the decrease in the PLQY for the delayed component in the temperature range 200–100 K should be considered due to both the suppression of triplet formation (*i.e.*, reduction of k_{ISC}) and a reduction of k_{RISC}. In fact, the temperature (200 K) coincides with the starting temperature of the decrease of the PLQY (delayed component) and the starting temperature of the nonlinear increase of the PLQY (for prompt emission).

Finally, we characterized the EL characteristics of the OLED using the **mCP : PO-T2T** or **mCP-d_{20} : PO-T2T** co-deposited layer as the emissive layer to evaluate the impact of donor-molecule deuteration on OLED performance. The donor-to-acceptor ratio in the co-deposited films was fixed at 9 : 1 because the blend ratio affects PL performance upon deuteration of the donor molecules, and the OLEDs employed the device structure shown in Fig. S7. No noticeable change in the current density–voltage characteristics was observed for both types of OLEDs, as shown in Fig. 3a. This observation is consistent with the results of the hole-only devices based on **mCP** and **mCP-d_{20}** (Fig. S8b). Although a previous study has reported that the deuteration of organic materials can provide higher charge transport properties in the solid-state film according to the change of the molecular density,[19] the **mCP** and **mCP-d_{20}** layers have almost the same hole transport ability in the device structure employed in this study, indicating that donor

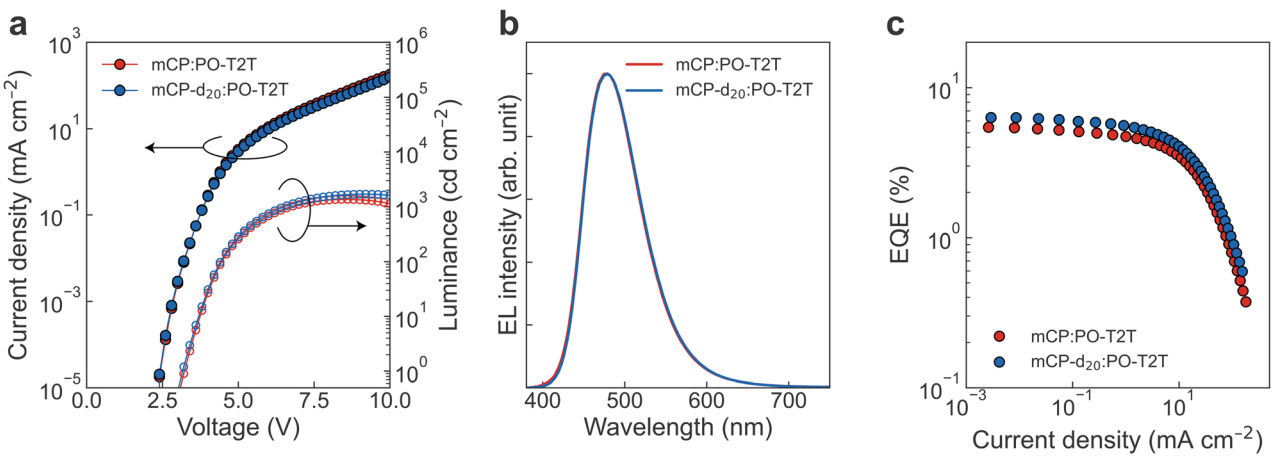

Fig. 3 (a) Current–voltage–luminance (*J*–*V*–*L*) curves, (b) EL spectra obtained at 8 V, and (c) EQE–*J* characteristics of the tested OLEDs.

deuteration does not affect the charge-transport properties in the OLEDs. In fact, although the film density of the **mCP-d_{20}** film increased from 1.111 ± 0.056 g cm^{-3} to 1.163 ± 0.085 g cm^{-3}, which was experimentally obtained using the same method as reported in previous studies,[19] this change mainly originated from the substitution with heavier deuterium atoms. In addition, as shown in Fig. 3b, no changes in the EL spectrum were observed in either type of OLED, in agreement with the steady-state PL results. Nevertheless, in the **mCP-d_{20}**:**PO-T2T**-based OLEDs, the maximum EQE and current efficiency were found to improve clearly (5.5% and 11.6 cd A^{-1} for the **mCP**-based OLED and 6.4% and 14.5 cd A^{-1} for the **mCP-d_{20}**-based OLED), as shown in Fig. 3c and Fig. S9, and these enhancements in the **mCP-d_{20}**:**PO-T2T**-based OLED should be attributed to the enhancement of the PLQY by deuteration of the **mCP** donor molecules. Although the **mCP-d_{20}**-based OLED exhibited a higher EQE than the **mCP**-based OLED, no significant change in operational stability was observed (Fig. S10). Note that our results do not mean that the deuteration of organic molecules does not affect the operational stability. The lack of a significant difference in operational stability observed in this study is likely due to the intrinsic low operational stability of the material combination (LT50 < 0.3 h for both OLEDs) and/or the limited impact of deuteration on operational stability, since only electron donors were deuterated.

Conclusion

In conclusion, to clarify the impact of deuteration of donor molecules in exciplex systems, the exciplex dynamics in the **mCP-d_{20}**:**PO-T2T** system were investigated in detail, including the kinetic analysis based on the temperature dependence of the related rate constants. We found that deuteration of donors in the exciplex system significantly reduces nonradiative decay from the triplet excited state, resulting in longer delayed fluorescence lifetimes and higher PLQYs compared to the **mCP**:**PO-T2T** system. Additionally, the deuteration effect becomes more pronounced as the proportion of deuterated donor molecules increases in the films (D:A ratio = 7:3–9:1), highlighting that the deuteration of surrounding molecules around emissive species is critical in addition to the deuteration of the emissive species. Furthermore, we find that the exciplex systems have activation energies for both ISC and RISC processes (~10 meV and ~46 meV, respectively), leading to an increase in the PLQY of the prompt fluorescent and a decrease in the delayed emission components with decreasing temperature. Further investigations, including the effect of acceptor deuteration, are expected to lead to a deeper understanding and further performance improvement of exciplex-based systems.

Experimental section

Materials and sample preparation

1,4,5,8,9,11-Hexaazatriphenylenehexacarbonitrile (**HAT-CN**), **mCP**, **PO-T2T**, and 8-hydroxyquinolinolato-lithium (**Liq**) were purchased from Luminescence Technology Corp. 9-Phenyl-3,6-bis(9-phenyl-9*H*-carbazol-3-yl)-9*H*-carbazole (**Tris-PCz**) and **mCP-d_{20}** were synthesized according to previously reported procedures. Organic thin films with a thickness of 50 nm for PL measurements were deposited onto quartz or silicon substrates by thermal evaporation under high vacuum conditions. The deposition was carried out under a vacuum of less than 2.0×10^{-4} Pa. For OLED fabrication, glass substrates patterned with 100 nm-thick indium–tin–oxide (ITO) electrodes were used. The substrates were sequentially cleaned by ultrasonication in neutral detergent, deionized water, acetone, and isopropanol. Residual moisture on the ITO electrodes was removed by boiling isopropanol vapor treatment, followed by drying under a nitrogen flow. Subsequently, the substrates were subjected to UV-ozone treatment for 15 min. The cleaned ITO substrates were immediately transferred into the vacuum deposition chamber, where organic and metal layers were successively deposited through appropriate shadow masks. After fabrication, the OLED devices were immediately encapsulated inside a nitrogen-filled glovebox (O_2 < 0.1 ppm, H_2O < 0.1 ppm) using glass covers coated with a moisture-absorbing material (Dynic Co., Ltd).

Optical characterization of organic thin films

Steady-state UV/vis absorption spectra were recorded with a UV–vis–NIR spectrophotometer (UV-3600i Plus, Shimadzu Corp.). Steady-state photoluminescence spectra were measured with a spectrofluorometer (FP3600, JASCO Co.) using an excitation wavelength of 300 nm. Photoluminescence quantum yields (PLQYs) were determined with an absolute PL quantum yield measurement system (Quantaurus-QY, Hamamatsu Photonics) at an excitation wavelength of 300 nm. The PLQY values were obtained as the average of three measurements using independent batches. Transient PL decay curves at room temperature were recorded using a fluorescence lifetime spectrometer (C16361-02, Hamamatsu Photonics). Temperature-dependent PL measurements were conducted using a fluorescence lifetime spectrometer (C16361-01, Hamamatsu Photonics) and a cryostat (CoolSpek, UNISOKU Co., Ltd). Time-dependent PL spectra were measured using a streak camera system (C4334, Hamamatsu Photonics) at an excitation wavelength of 355 nm.

OLED characterization

The current density–voltage–luminance (*J*–*V*–*L*) characteristics of the OLEDs were evaluated using a source meter (Keithley 2400, Keithley Instruments, Inc.) and a calibrated luminance meter (CS-2000A, KONICA MINOLTA). All device measurements were performed in ambient air at room temperature.

Author contributions

The project was conceived and designed by Y. N. and H. N. Y. N. prepared the samples and measured their properties. Y. N. and H. N. analyzed all the data collected in this study. All authors

contributed to writing the paper and provided critical comments on the project.

Conflicts of interest

The authors declare no conflicts of interest.

Data availability

The data supporting the findings of this study are available within the article and its supplementary information (SI). Supplementary information is available. See DOI: https://doi.org/10.1039/d5tc04017e.

Additional raw data files are available from the corresponding author upon reasonable request.

Acknowledgements

The authors thank Ms Yuika Tamura of Kyushu University for preparing the chemicals. This work was partially supported financially by the Japan Society for the Promotion of Science (JSPS) KAKENHI (Grant Numbers 23H05406, 23K17367, 23K20039, and 25K01847).

References

1 M. A. Baldo, D. F. O'Brien, A. Shoustikov, S. Sibley, M. E. Thompson and S. R. Forrest, *Nature*, 1998, **395**, 151–154.
2 B. Minaev, G. Baryshnikovb and H. Agrena, *Phys. Chem. Chem. Phys.*, 2014, **16**, 1719–1758.
3 A. Endo, M. Ogasawara, A. Takahashi, D. Yokoyama, Y. Kato and C. Adachi, *Adv. Mater.*, 2009, **21**, 4802–4806.
4 H. Uoyama, K. Goushi, K. Shizu, H. Nomura and C. Adachi, *Nature*, 2012, **492**, 234–238.
5 C.-Y. Chan, M. Tanaka, Y.-W. Wong, H. Nakanotani and T. Hatakeyama, *Nat. Photon.*, 2021, **15**, 203–207.
6 K. Goushi, K. Yoshida, K. Sato and C. Adachi, *Nat. Photon.*, 2012, **6**, 253–258.
7 Y.-S. Park, S. Lee, K.-H. Kim, S.-Y. Kim, J.-H. Lee and J.-J. Kim, *Adv. Funct. Mater.*, 2013, **23**, 4914–4920.
8 B. Liang, J. Wang, Y. Cui, J. Wei and Y. Wang, *J. Mater. Chem. C*, 2020, **8**, 2700–2708.
9 J. Sun, H. Ahn, S. Kang, S.-B. Ko, D. Song, H. A. Um, S. Kim, Y. Lee, P. Jeon, S.-H. Hwang, Y. You, C. Chu and S. Kim, *Nat. Photon.*, 2022, **16**, 212–218.
10 H.-T. Cao, P.-F. Hou, W.-J. Yu, Y. Gao, B. Li, Q.-Y. Feng, H. Zhang, S.-S. Wang, Z.-M. Su and L.-H. Xie, *ACS Appl. Mater. Interfaces*, 2023, **15**, 7236–7246.
11 R. Englman and J. Jortner, *Mol. Phys.*, 1970, **18**, 145.
12 S.-F. Wang, B.-K. Su, X.-Q. Wang, Y.-C. Wei, K.-H. Kuo, C.-H. Wang, S.-H. Liu, L.-S. Liao, W.-Y. Hung, L.-W. Fu, W.-T. Chuang, M. Qin, X. Lu, C. You, Y. Chi and P.-T. Chou, *Nat. Photonics*, 2022, **16**, 843.
13 Y.-C. Wei, K.-H. Kuo, Y. Chi and P.-T. Chou, *Acc. Chem. Res.*, 2023, **56**, 689.
14 S. Wang, D. Zhou, K. Kuo, C. Wang, C. Hung, J. Yan, L. Liao, W. Hung, Y. Chi and P. Chou, *Angew. Chem., Int. Ed.*, 2024, **63**, 202317571.
15 T. Huang, Q. Wang, H. Zhang, Y. Zhang, G. Zhan, D. Zhang and L. Duan, *Nat. Photon.*, 2024, **18**, 516–523.
16 Q. Yu, Y. Tamura, H. Nakanotani, M. Mamada and C. Adachi, *Adv. Opt. Mater.*, 2024, **12**, 2400932.
17 P. Wang, F.-F. Wang, Y. Chen, Q. Niu, L. Lu, H.-M. Wang, X.-C. Gao, B. Wei, H.-W. Wu, X. Cai and D.-C. Zou, *J. Mater. Chem. C*, 2013, **1**, 4821–4825.
18 H. Tsuji, C. Mitsui and E. Nakamura, *Chem. Commun.*, 2014, **50**, 14870–14872.
19 X. Liu, C.-Y. Chan, F. Mathevet, M. Mamada, Y. Tsuchiya, Y.-T. Lee, H. Nakanotani, S. Kobayashi, M. Shiochi and C. Adachi, *Small Sci.*, 2021, **1**, 2000057.
20 W. Li, A. Wu, T. Fu, X. Gao, Y. Wang, D. Xu, C. Zhang, Z. Sun, Y. Lu, D. J. Young, H. Li and X.-C. Hang, *J. Phys. Chem. Lett.*, 2022, **13**, 1494–1499.
21 J. Yao, S. C. Dong, B. S. T. Tam and C. W. Tang, *ACS Appl. Mater. Interfaces*, 2023, **15**, 7255–7262.
22 W. Yuan, T. Huang, J. Zhou, M.-C. Tang, D. Zhang and L. Duan, *Nat. Commun.*, 2025, **16**, 4446.
23 M. Morgenroth, T. Lenzer and K. Oum, *J. Phys. Chem. C*, 2023, **127**, 4582–4593.
24 J.-H. Lee, S.-H. Cheng, S.-J. Yoo, H. Shin, J.-H. Chang, C.-I. Wu, K.-T. Wong and J.-J. Kim, *Adv. Funct. Mater.*, 2015, **25**, 361–366.
25 Y. Tsuchiya, S. Diesing, F. Bencheikh, Y. Wada, P. L. d Santos, H. Kaji, E. Z.-Colman, I. D. W. Samuel and C. Adachi, *J. Phys. Chem. A*, 2021, **125**, 8074–8089.
26 M. Zhang, K. Wang, C.-J. Zheng, D.-Q. Wang, Y.-Z. Shi, H. Lin, S.-L. Tao, X. Li and X.-H. Zhang, *Front. Chem.*, 2019, **7**, 16.
27 K.-H. Kim, S.-J. Yoo and J.-J. Kim, *Chem. Mater.*, 2016, **28**, 1936–1941.